A NOVEL TYPE OF MULTI-EVAPORATOR CLOSED LOOP TWO PHASE THERMO-SYPHON: THERMAL PERFORMANCE ANALYSIS AND FLUID FLOW VISUALIZATION

M. Mameli[a,c*], mauro.mameli@unibg.it
D. Mangini[a], daniele.mangini@unibg.it
G.F. Vanoli[b], giulio.vanoli@mail.polimi.it
L. Araneo[b], lucio.araneo@polimi.it
S. Filippeschi[c], sauro.filippeschi@den.unipi.it
M. Marengo[a,d], M.Marengo@brighton.ac.uk

[a] Dept. of Engineering and Applied Sciences, University of Bergamo, Viale Marconi 5, 24044 Dalmine (BG), Italy
[b] Politecnico di Milano, Dipartimento di Energia, Via Lambruschini 4A, 20158 Milano, Italy
[c] Università di Pisa, DESTEC, Largo Lazzarino 2, 56122 Pisa, Italy
[d] School of Computing, Engineering and Mathematics, University of Brighton, BN2 4GJ, Brighton,,UK.

ABSTRACT

A novel type of multi-evaporator Closed Loop Two Phase Thermosyphon has been designed and tested at different inclinations and heat input levels. The device consists in an aluminum tube (I.D./O.D. 3/5mm), bent into a planar serpentine with five U-turns in the heated zone, with a 50 mm transparent section for the purpose of visualization. The tube is closed in a loop, evacuated and partially filled with FC-72, 50% vol. Five electrical heating wires are wrapped on the U-turns, providing a symmetrical heating to the device. The condenser zone is embedded into a heat-sink and cooled by fans blowing air at 22°C. Sixteen T-type thermocouples are located on the external tube wall in the evaporator and condenser zones, while the fluid pressure is measured in the condenser zone adjacent to the transparent tube. The flow pattern is recorded by means of a high-speed camera, the device operational limits (start-up and dry-out heating levels at the different inclinations) are detected and the overall thermal performance is calculated. The vertical operation shows the most promising results since the device is able to dissipate heat fluxes up to 13.5 W/cm^2 and keeps the evaporator zone below 85°C.

INTRODUCTION

Two-phase heat transfer devices have always been attractive for their compactness, high performance and, above all, the possibility of being completely thermally driven (passive). The increasing need of managing high heat fluxes, either to be dissipated (electronics cooling) or to be recovered (solar concentrators), drives towards the design of more efficient and reliable devices. Despite the last decades witnessing the overwhelming spread of heat pipe technology under various forms, such as grooved and sintered heat pipes, loop heat pipes and capillary pumped loops, the interest in wickless, gravity driven technologies, namely the Two Phase Thermosyphons (TPTS), never damped out. The capability to transport heat at high rates over appreciable distances, without any requirement for external pumping devices, the low cost, durability and relatively simpler modeling/design process make this technology very attractive for different thermal management applications. Indeed, TPTS have been studied for nuclear plants (Lahey and Moody, 1993), energy systems (Franco and Filippeschi, 2013), solar heat recovery (Esen and Esen, 2005), (Li et al., 2014), (Moradgholi et al., 2014), air conditioning (Han et al., 2013), avionics (Sarno et al., 2013), railway traction (Perpinà et al., 2007) and electronic cooling applications (Jouhara and Robinson, 2010). The typical TPTS (Reay and Kew, 2006) consists of a single envelope where the heat-receiving (evaporator) zone is usually filled with the liquid phase and it is located below the heat rejecting (condenser) zone. As the evaporator zone is heated up the liquid starts boiling and vapor rises and condenses on the walls in the heat-rejecting zone. The liquid film flows down the walls to the evaporator zone counter-current the vapor. Nevertheless, this device can also be arranged in a loop configuration, to better assist the two-phase flow motion both in the condenser and in the evaporator zone (Kaminaga et al., 2012), (Kim et al., 2005). Especially for the electronic cooling, the loop thermosyphons are largely investigated because of their geometrical flexibility in the design of the evaporator and the condenser zones with respect to a single straight channel typical of a normal thermosyphon (Franco and Filippeschi, 2012).

The present device is designed especially to meet electronic requirements: it consists in a relatively small diameter aluminum tube (3 mm ID, 5 mm OD), however higher than the capillary diameter for the used refrigerant (1.6 mm for FC-72 at 20 °C). As thoroughly described by Franco and Filippeschi (2010), thanks to the relatively small cross section with respect to the standard TPTS, the expanding vapor phase is able to push batches of fluid (both liquid and vapor) towards the condenser section. This particular fluid flow motion is better known as "bubble lift" principle. In the cooled zone, vapor condenses and the tube is completely filled by the liquid phase that is driven back to the evaporator by gravity. The looped TPTS based on the "bubble lift" concept, exploits the higher heat transfer performance linked to the convective flow boiling process. Indeed, the tube is bended in a serpentine, with 5 U-turns at the evaporator zone. Every turn is heated up by means of a heating wire, expanding the above concept into a multi evaporator two-phase loop. The transparent section (50 mm axial length) in the condenser zone allows visualizing the fluid and creating a flow pattern matrix with respect to the different heat input and inclination levels. Indeed, the objective of the work is not only to provide quantitatively the thermal performance of this new kind of multi evaporator thermosyphon (under different heat power input levels and different inclination angles), but also to establish a relation between the thermal behavior and the fluid flow motion.

EXPERIMENTAL SETUP AND PROCEDURE

The proposed cooling device is made of an aluminum tube (I.D./O.D. 3.0 mm/5.0 mm) bent into a planar serpentine with ten parallel channels and five turns at the evaporator (all curvature radii are 7.5 mm), as shown in Figure 1a. The aluminum tube is filled up with a refrigerant fluid (FC72), utilizing a FR=50%, corresponding to 8.3 ml. The thermosyphon has been tested at different heat loads from 10 W up to 260 W and different inclination angles (vertical, 75°, 60°, 45°, 30°, 15°, 5°, 2.5°, horizontal). A 50 mm glass tube closes the loop at the top of the condenser zone, allowing the flow pattern visualization. The glass tube is connected to the aluminum serpentine by means of two "T" junctions that derive two ports at each side: one is devoted to the vacuum and filling procedures, while the second one hosts a pressure transducer (Kulite®, XCQ-093, 1.7 bar A, Accuracy 0.5% FSO).

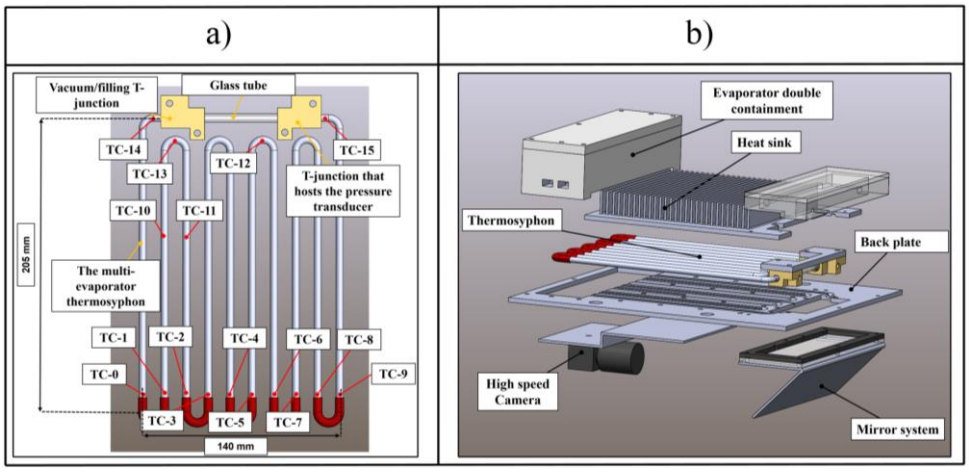

Figure 1: a) Thermocouples and heaters location along the thermosyphon tube; b) Exploded view of the test cell with all its components. The heating zone is highlighted in a red colour in both of the figures.

Sixteen "T" type thermocouples (bead diameter 0.2 mm, ± accuracy 0.3 K) are located on the thermosyphon external tube wall: ten in the evaporator zone and six in the condenser zone, while an additional thermocouple is utilized to measure the ambient air temperature as illustrated in Figure 1a. A low vapor pressure glue (Varian Torr Seal®) seal together the aluminum tube, the "T" junctions and the glass tube.

The exploded view of the test cell, with its main components, is shown in Figure 1b. A compact camera (Ximea®,MQ013MG-ON, objective: Cosmicar/Pentax® C2514-M) records the fluid regimes. The camera, reducing the region of interest only at the glass tube, acquires images up to 450 fps with a resolution of 1280x162 pixel (25 pixel/mm). The thermosyphon is firstly evacuated by means of a vacuum system (Varian® DS42, TV81-T) down to 10^{-6} mbar. Before filling up, the incondensable gases are earlier removed by continuous boiling and vacuum cycles in a secondary tank, as described by Henry et al. (2004). Finally, the system is filled up with the working fluid (FC-72) with a volumetric ratio of 0.5 ± 0.02. The difference between the actual fluid pressure inside the tube and its saturation pressure, at the ambient temperature, gives an indication of the incondensable gas content. For the present case this difference is less than the pressure transducer accuracy. Five electrical heaters (Thermocoax® Single core 1Nc Ac, 0.5 mm O.D., 50 Ω/m, each wire is 720 mm long) are wrapped on the evaporator U-turns (Figure 1) covering a tube portion of 40 mm. A power supply (GWInstek® 6006A) is connected to the heaters, providing an electric power input up to 260 W (corresponding to a wall to fluid radial heat flux of 13.5 W/cm^2). Steady state conditions can be reached in approximately 3 minutes due to the low thermal inertia of the heating system. The thermosyphon heat sink is cooled down by means of two air fans (Sunon® PMD1208PMB-A), positioned just above it (165 mm total length), as shown in Figure 2a. To increase the cooling surface exposed to ambient convection, the condenser is embedded between a heat sink and a back plate (Figure 2b) where circular cross section channels are milled. The thermal contact between the heat sink, the aluminum back-plate and the thermosyphon is increased with a heat sink compound (RS® Heat Sink Compound). All the tests are performed at ambient temperature (22 °C ± 1.5 °C). The cooling device, the thermocouples, the pressure transducer, the heating and cooling system as well as the visualization system are placed on a structure that can be easily tilted from the vertical position (bottom heat mode) to the horizontal. The thermocouples and the pressure transducer outputs are recorded by a data acquisition system (NI-cRIO-9073®, NI-9214®, NI-9215®) at 16 Hz. A video (10 seconds at 450 fps) is recorded during each heat input power level for all the inclination angles. Even though pseudo-steady conditions are reached in approximately 3 minutes, the video recording starts 13 minutes after every heat power input variation in order to be sure to measure in pseudo-steady state conditions during the flow pattern recording.

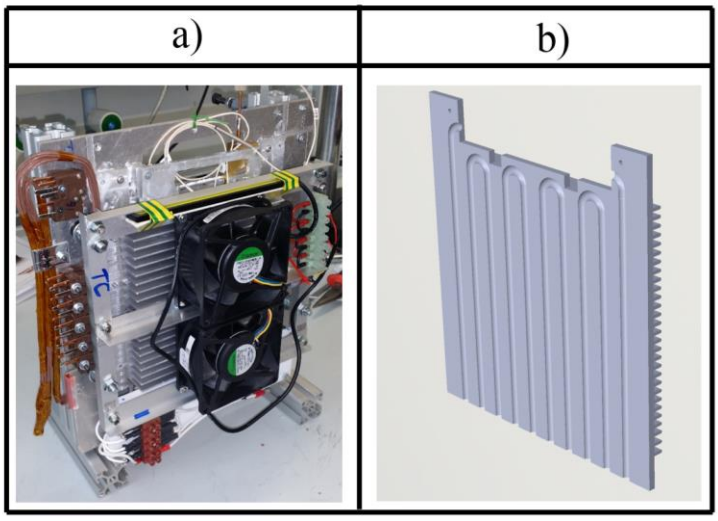

Figure 2: a) The two fan mounted above the heat sink; b) CAD view of the milled heat sink.

THERMAL CHARACTERIZATION

The experimental campaign is carried on in order to identify:

- the temporal evolution of the tube temperature in every branch of the evaporator zone and along the condenser zone;
- the operation regimes in terms of fluid motion;
- the operational limits in terms of heat input levels and orientation;
- the device thermal performance at each input level and orientation.

For each inclination, the heater input power is increased in multiples of 10 W steps, with finer detail in the low power region, until a thermal crisis condition (namely the evaporator dry-out condition) is reached. After the sudden increase of the evaporator temperatures due to the dry-out condition, at the following power step the heating power is reduced and the thermal characterization is continued while decreasing the heat input levels. Each power step is maintained for 15 minutes so that the system can reach a steady state condition and the equivalent thermal resistance can be evaluated as follows (Eq. 1):

$$R_{eq} = \Delta\overline{T}_{e-c} / \dot{Q} \tag{1}$$

where $\Delta\overline{T}_{e-c}$ is the difference between the evaporator and the condenser mean temperatures, averaged in time during the last minute of the pseudo-steady state, and $\dot{Q}$ is the heat power input provided to the evaporator zone by the five heaters. Care is taken to allow the liquid residing evenly among the curves by holding the device horizontal before raising it back to the desired inclination.

Thermal characterization in vertical position

Figure 3 shows the temperature evolution of the tube wall temperatures in several locations:

- the red/yellow and violet lines indicate the temporal evolution of the temperatures in the evaporator zone just above the heater (TC0, TC1, TC2, TC3, TC4, TC5, TC6, TC7, TC8, TC9);
- the temperatures recorded in the condenser zone are illustrated with blue color variations (TC10, TC11, TC12, TC13, TC14, TC15);
- the ambient temperature is visible in green.

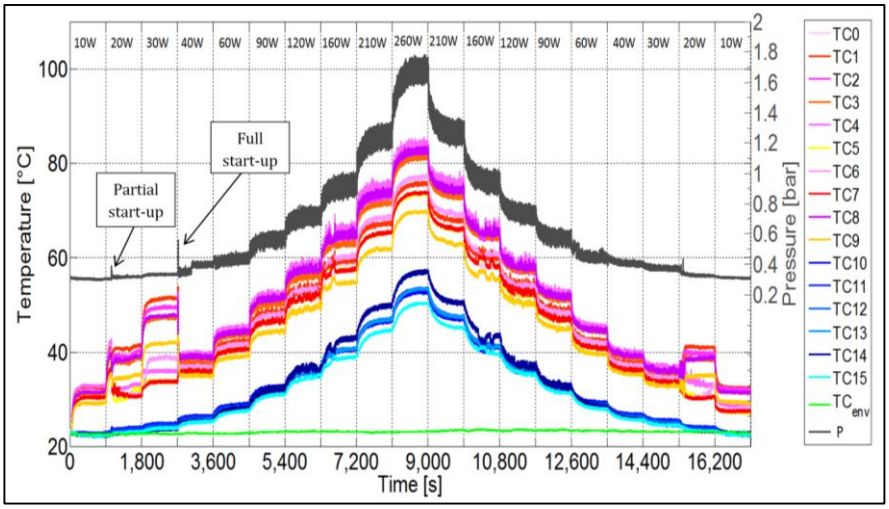

Figure 3: Temperature and power input diagram in vertical position.

The secondary y-axis on the right side corresponds to the fluid pressure level, while the sequence of the heat input levels is indicated at the upper side of the chart. During the first heat input levels (up to 20 W) the fluid is not moving, as evidenced by the smooth pressure signal, and heat is transferred mostly by pure conduction along the tubes. For this reason, even small differences in the thermal contact between the five heating wires and the tube portions can cause a 10°C temperature spread within the evaporator zone. At 20 W (corresponding to a heat flux of ≈1 W/cm^2) the fluid motion is activated only in some channels, again probably due to the unavoidable minimal hardware differences in the thermal contact between the heating wires and the tube wall (partial start-up in Figure 3). The pressure signal in the condenser zone points out a sudden peak while the temperatures recorded by TC4 to TC7 (the ones placed on the third and fourth U-turns from the left in Fig. 1a), pushed from the evaporator zone, is suddenly visible in the glass tube in the condenser zone. Also at 30 W a partial start-up is evident: the temperature distribution in the evaporator zone occupies a wide range of approximately 20 °C, pointing out the fluid flow motion in some channels, and a lack thereof in others. At 40W, the device starts-up and the regime switches from stationary to oscillating almost instantaneously, resulting in a sharp decrease of all heater temperatures and a noticeable narrowing of the evaporator temperature distribution. Indeed, in vertical position the combined effect of vapor bubble-lift and gravity helps the fluid rising up from the evaporator and descending immediately in the condenser. Thusly the device continues to work without dry-out up to the power supply limit of 260 W, corresponding to a tube to fluid radial heat flux of 13.5 W/cm^2, maintaining the evaporator temperature below 85 °C. During power-down, the fluid motion is maintained even at 30 W. The device activation, occurring at different heat input levels during the power-up and power-down periods, depends on the heating history (increasing/decreasing heat power levels) at least for the first ramp-up power increases, and questions about such possible hysteresis rise: what if the heat input level is again increased? Would the device operation be activated again at 40 W, proving the existence of hysteresis? Or does the flow motion follows the last registered trend, activating at 20 W, testifying only a single start-up phenomenon? In order to answer to the previous questions additional tests are performed with three subsequent heating ramps. The device is first heated up at 10 W, 20 W, 30 W, 40 W and 80 W; then it is powered down following the same steps to 10 W and finally heated up another time at 80 W. Like the other tests, every power step is held for 15 minutes in order to reach steady state conditions and thus have the possibility to calculate $R_{eq.}$. Figure 4 shows the equivalent thermal resistances in three different power ramps: first power-up (Q_{up}), subsequent power-down through the same power steps (Q_{down}) and then second power-up again through the same heating levels (Q_{up2}).

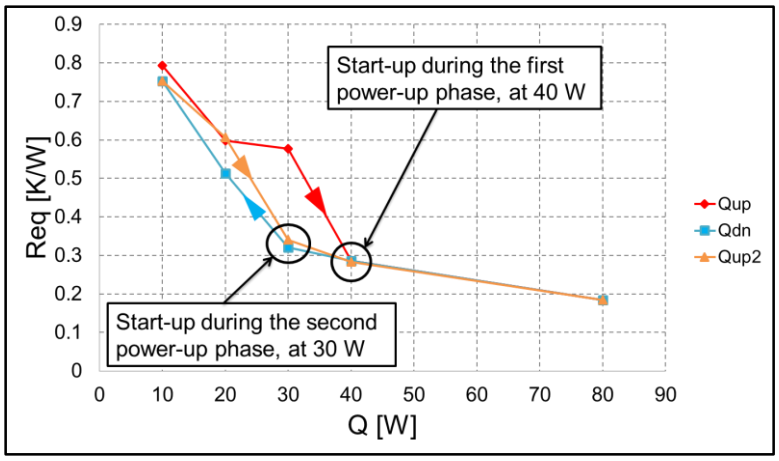

Figure 4: Equivalent thermal resistance during the hysteresis detection test.

During the first power-up phase the device start-up is easily recognized in terms of thermal performance by the sudden decrease of the equivalent thermal resistance occurring at 40W (blue line) since at 30W no regular fluid motion is detected. At 80 W the fluid motion is fully activated and, during the power-down phase, a residual oscillation is still detected also at 30 W, resulting in a lower thermal resistance with respect to the power-up case. Because the equivalent thermal resistance trend related to second power-up (green line) nearly overlaps to the one related to the power-down (red line), it can be concluded that the device undergoes a single start-up issue and not a real hysteresis. This could be explained as follows: the Q_{up2} case starts from a higher energized situation than the Q_{up}. The nucleation sites, already vigorously activated by the first two ramps (Q_{up} and Q_{down}), are not completely de-activated when the Q_{up2} starts. This situation causes an earlier start-up in the Q_{up2}, allowing the two-phase fluid to move even at 30 W.

Effect of orientation

After the vertical test, other tests at 75 °, 60°, 45°, 30°, 15°, 2.5° and another one leaving the device horizontally are performed to evaluate the effect of inclination on the thermal performance of the device. Results are shown in Figure 5a for the power-up case and 5b for the power-down case. In light of the start-up test results, the thermal resistance values registered during the first power-up are only indicative of the device's behavior at start-up. The fact that the liquid phase returns to the condenser more efficiently when the device is fully assisted by gravity (vertical operation) is not valid for the start-up phase, as already shown for other looped two phase passive devices (Mameli et al., 2013). In fact, one might expect the device start-up to occur at lower heat input levels for lower inclinations, but looking at figure 5a, it is evident that the start-up heat input ranges from 30 W to 90 W, without a univocal dependence on the tilting level. On the other hand, in the power-down case (Fig 5b), the fluid motion remains active down to 30 W for all the inclinations, meaning that the liquid phase is pushed back to the condenser more efficiently only when the gravity effect is coupled with fluid inertial effects or, in other words, when the flow motion has already been activated. Therefore, once start-up is achieved and even a small amount of heating power is provided which keeps the nucleation sites active, the power-down phase is a better representation of actual operative performance and can be further examined to distinguish a power range where the device exhibit a stable operation from one where thermal crisis conditions begin to manifest.

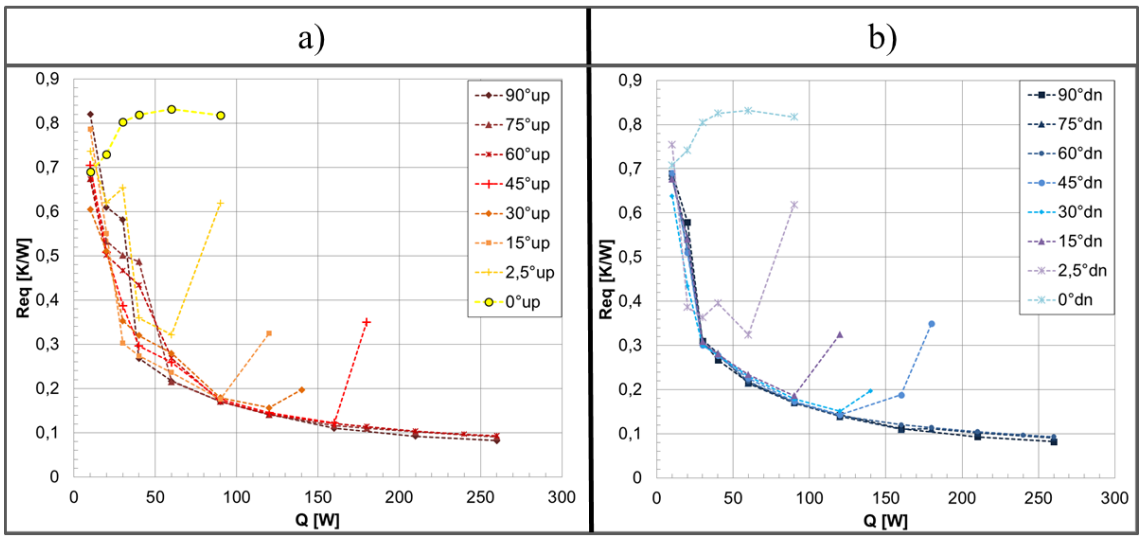

***Figure 5**: Equivalent thermal resistance at various inclinations. a) The first power-up; b) The subsequent power-down.*

In the horizontal position, there is no gravitational head between evaporator and condenser. Furthermore, since the tube diameter is larger than the capillary limit (almost 1.6 mm for FC-72 at 20°C), the liquid phase always resides in the lower half of the pipe while the vapor phase in the upper one: fluid motion is not assisted by gravity and vapor is never confined between liquid batches. This results in a complete absence of macroscopic fluid motion for all the tested heat input levels; the heat transfer is mainly due to conduction within the tube wall and the fluid itself and the equivalent thermal resistance remains constant after reaching the maximum value of 0.8 K/W. This trend is taken as reference point because it basically states that the device is not working as a two-phase heat transfer device.

A slight inclination with respect to the horizontal position (2.5°) is sufficient to assist the fluid motion: the rising bubbles flatten against the upper side of the tubing and, despite the bubble lift effect being drastically reduced, vapor is able to slide upwards and contribute to convective cooling. Indeed both during power-up and power-down the fluid starts oscillating at 20 W. For all the inclinations at the lowest power output setting, 10 W, the system always shows its highest thermal resistance (between 0.6 K/W and 0.8 K/W) because the heating power is never sufficient to activate the fluid motion inside the device, and the heat transfer is mainly due to pure conduction. At medium-low power heat power inputs (the normal operation range in figure 5b), all experiments (except the test done with an inclination of 2.5°, which is too low to achieve a stable operation) show the same performance trend: after activation, the curves collapse into a narrow band of thermal resistance values and the performance can therefore be considered independent of inclination. This indicates that when fluid motion is strong, the inertia of the circulating fluid is much more relevant than the effect of inclination. As power is increased, equivalent thermal resistance values continue to gradually decrease until the power supply limit or a thermal crisis condition are reached, causing temperatures in the affected sections to rise over 100°C, noticeably penalizing the thermal performance. When the heat flux locally exceeds the CHF, a local dry-out condition occurs meaning that a vapor film forms preventing contact between liquid and heated surface. The resulting loss of heat transfer capability causes the local temperature to rise again over 100°C. The dry-out, which abruptly increases the temperatures in the evaporator zone, causes a significant increase of the R_{eq}. The inclination angle plays an important role for the dry-out. At 15°, the dry-out conditions are reached at 120 W of heat power input. Increasing the inclination angle to 30° and then 45°, the working-mode range continues to expand up to 180 W. For the highest inclination angles tested (60°, 75° and vertical position) the device works up to the limit of the power supply, arriving at 260 W without reaching thermal crisis. Increasing the inclination angle allows gravity to better assist the downflow of the liquid batches from the condenser to the evaporator section, facilitating its cooling. This eventually leads the device to exhibit performance values lower than 0.1 K/W regarding the R_{eq} at the highest inclination.

Stable operation: Oscillation VS Circulation

After the thermal-hydraulic activation, the fluid flow motion is observable through the glass tube in the condenser zone. In particular, two working modes can be recognized: one where the fluid is only oscillating through the channels and the second one with a constant circulating component. Figure 6a shows a sequence of images taken during the experiment done in vertical position when the heat power input was set at 120 W. The different bubbles that pass through the transparent section are highlighted with different colors to distinguish them across the sequence of images. The two-phase flow motion does not follow a preferential direction during its motion within the loop, but oscillates randomly: e.g. the large bubble A in Figure 6a at a certain point stops and abruptly changes flow direction from the right to the left. As a consequence, the temperatures at the edges of the glass tube (measured by the TC 14 to the left and TC 15 to the right) do not assume a monotone trend. When, for example, the oscillation goes from the left to the right, the temperature to the left will increase, while the temperature on the right will decrease and vice-versa in case of inverted motion as shown in figure 6c. The fact that the oscillation is the most common working mode observed is due to the symmetrical position of the heaters in the evaporator zone: there, the five electrical resistances are wrapped directly on the U-turns, thus the heat power input is equally distributed in all the branches of the device. Since the heat power input is the pumping force of a thermosyphon, the part of the device in contact with the heaters could be assimilated mechanically to pistons in parallel that together push the liquid and vapor phases in the condenser zone. This means that the two-phase flow is pushed in the condenser zone with the same driving force in all the branches of the device, making the fluid flow motion fluctuating and thus obstructing a fluid flow motion in a preferential direction. Despite this, for the highest inclination angles tested (vertical, 75°, 60°), a fluid motion in a preferential direction is also recognizable from 160 W to 260 W as shown in Figure 6b, where all the bubbles are moving in the same direction. As a consequence, the temperatures measured by TC 14 and TC15 both decrease continuously until steady state conditions are reached, as shown in Figure 6d.

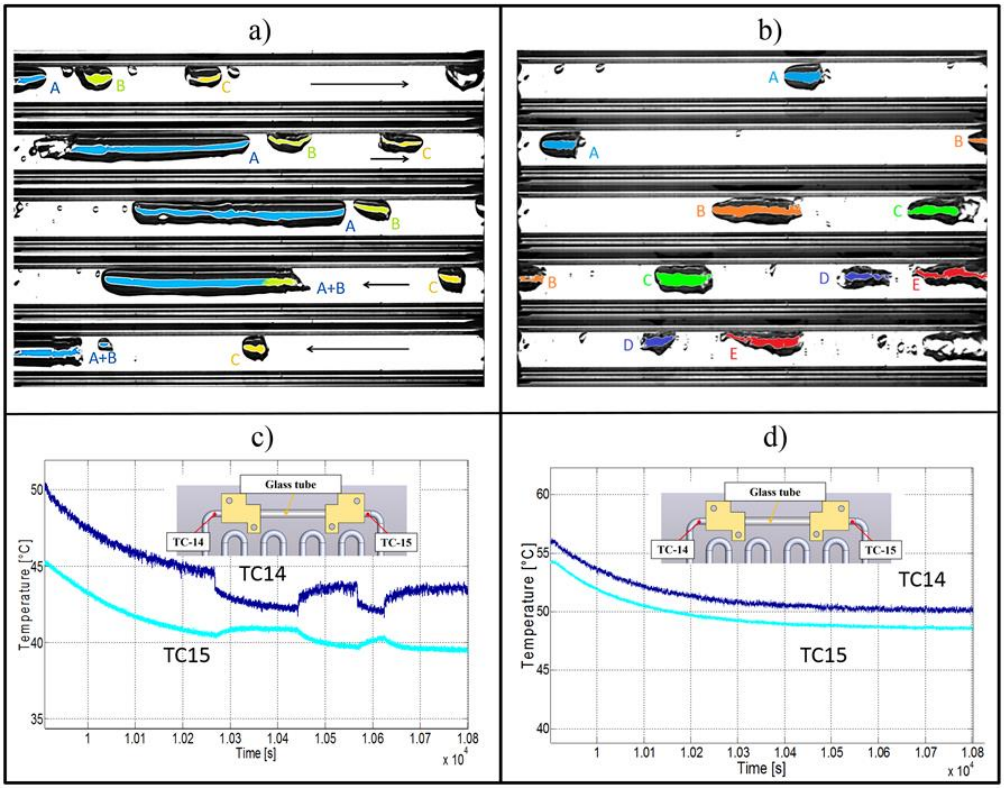

Figure 6 a) Two-phase flow oscillation in vertical orientation at 120 W power input (shown at 28 FPS); b) Two-phase flow circulation at 75° inclination and 210 W power input (shown at 45 FPS); c) TC14 and TC15 values during oscillation; d) TC14 and TC 15 values during circulation.

At the highest heat power inputs, when the two-phase flow is pumped to the condenser most forcefully, even the smallest asymmetries typical of an experimental set-up, or a particular distribution of the mass of fluid between the U-turns can cause the fluid motion to follow a preferential direction. This changes the motion from oscillating to circulating, improving consequently the convective heat transfer component. Indeed, for these high inclination angles the device is able to dissipate 260 W without reaching any kind of thermal crisis with an equivalent thermal resistance lower than 0.1 K/W. Another important consideration during stable operation is that, in the power-down case, the fluid flow remains active for lower heat power inputs than those of the start-up phase. This means that the liquid phase is pushed back to the condenser more efficiently only when the gravity effect is coupled with fluid inertial effects or, in other words, when the flow motion has already been activated.

VISUALIZATION AND FLOW PATTERN MAP

During the device operation, four different flow regimes were observed and distinguished through the transparent tubing section; they are listed in Table 1 with the following symbols:

- "-" = no fluid motion;
- "S" = start-up, shut-down (unstable): flow can be stratified or weakly oscillating, with partial activation or deactivation of some heated sections;
- "O" = oscillating (stable): a strong movement of fluid oscillating back and forth;
- "C" = circulating (stable): a strong movement of fluid in one specific preferential direction;
- "D" = dry-out: when excessive heat power input causes a thermal crisis in at least one evaporator section.

Table 1: Observed flow conditions at varying degrees of inclination and power output. Empty fields are untested power levels and behavior is inferred.

Power-up phase (Q up)														Power-down phase (Q down)											
90°	-	-	-	S	O	O	O		O		C		C		C		O		O	O	O	S	-	-	-	90°
75°	-	-	-	-	O	O	O		C	C	C		C		C	C	O		O	O	O	O	O	-	-	75°
60°	-	-	-	-	O	O	O		C	C	C	C	C	C	C	C	O		O	O	O	S	S	-	-	60°
45°	-	-	O	O	O	O	O		O	D						D	O	D	O	O	O	S	S	-	-	45°
30°	-	-	S	O	O	O	O	D									D	O	O	S	-	-	-	-	-	30°
15°	-	-	S	S	O	O	D											D	O	O	O	O	-	-	-	15°
2.5°	-	S	S	S	O	D													D	O	O	O	S	-	-	2.5°
0°	-	-	-	-	-	-													-	-	-	-	-	-	-	0°
P[W]	10	20	30	40	60	90	120	140	160	180	210	240	260	240	210	180	160	140	120	90	60	40	30	20	10	P[W]

Table 1 shows how an increase in inclination, and thus gravitational assistance, broadens the operative range of the device. Before the start up and during the shutdown, the other two characteristic flow types are stratified flow (Figure 7a), where fluid speed and direction are only assessable from ripples that run along the liquid-vapor interface, and the oscillating bubble (Figure 7b). This last kind of motion is seen mostly during power-down: a single, elongated bubble oscillates back and forth in the condenser zone. In this condition, thermal resistance values still remain relatively low than 0.3 K/W. When there is no fluid motion in the condenser, the glass tube is completely empty as visible in Figure 7c.

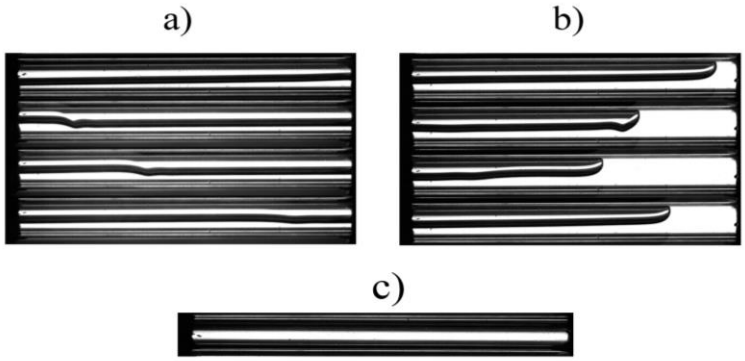

Figure 7 Exempla of fluid patterns in the tube, a) Stratified flow at approximately 50 FPS; b) Oscillating flow at approximately 50FPS; c) Empty tube.

Other interesting fluid flow phenomena are observed in the transparent section during tests, such as trailing edge break-up of the bubbles (Figure 8a) and condensation of the vapor phase (Figure 8b). During pulsations (and circulation for the highest heat power inputs), larger bubbles travel fast enough that their trailing edge breaks up into smaller bubbles, as shown in Figure 8a, which shows a sequence of images collected during a test in vertical orientation with 160 W of heat power input. The kinetic effects are so strong that the shear stress forces breaks the trailing edge, dividing it into smaller bubbles.

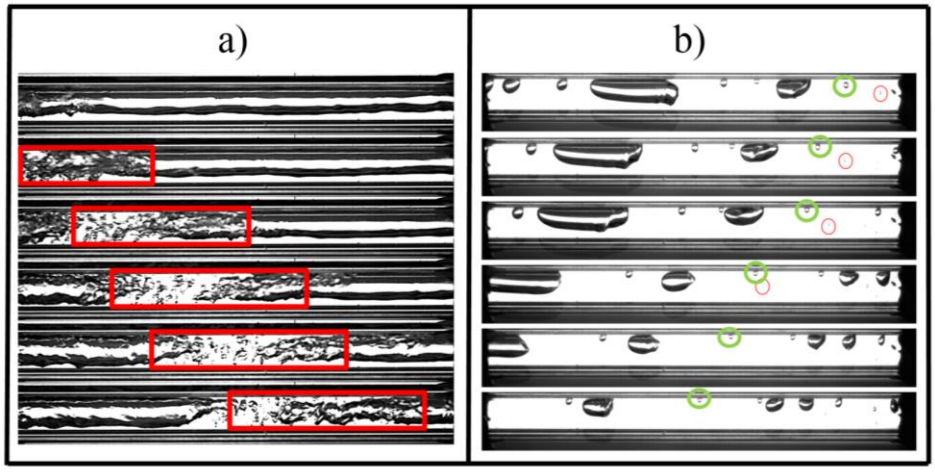

Figure 8. a) Trailing edge break-up and its division in smaller bubbles shown at 150 FPS (160 W, 90°); b) Bubble condensation phenomena observed along the transparent section shown at 80 FPS (80 W, 90°).

These smaller bubbles visibly shrink as the vapor condenses, as shown in Figure 8b, taken during the test in vertical orientation at 80 W, the condensation of the smallest bubbles that transit inside the tube is clearly visible (highlighted in red and green to better understand their motion in the sequence). This sequence of images points out that not only does the vigorous motion of the two-phase flow play an important role in the heat exchange, but also how latent heat is rapidly released during phase transition.

CONCLUSIONS

For the first time in literature, a multi-evaporator, closed loop thermosyphon is tested. The device is made by a 3mm ID aluminium tube with 5 U-turns at the evaporator zone, partially filled with liquid FC-72 (50% FR). A glass tube completes the loop in the condenser zone, allowing fluid flow visualization. A set of sixteen thermocouples is utilized to thermally characterize the device, while the inner pressure of the thermosyphon is measured by a miniaturized pressure transducer placed in the condenser zone, directly in contact with the fluid. The heat sink is cooled externally using ambient temperature air. The main results are:

- The device does not exhibit hysteresis between power-up and power-down, but instead experiences penalized performance during the first start-up from cold conditions. Once activation is achieved, power-up and power-down phases show similar performance.
- There is no univocal dependency between the tilting angle and the start-up heat input level. On one hand, increasing the inclination angle allows the "bubble lift" effect to better push the liquid phase into the condenser zone. On the other hand, decreasing the inclination angle, the height difference between the evaporator and the condenser is decreased, which also decreases the driving force needed to reach the top of the condenser.
- Once the device is activated, the thermal performance increases with power: above 3.3 W/cm^2, the equivalent thermal resistance drops below 0.34 K/W, reaching values of 0.1 K/W at 13.5 W/cm^2 in vertical conditions.
- The liquid phase is pushed back to the condenser more efficiently only when the gravity effect is coupled with fluid inertial effects: in the power-down phase, where fluid motion is already active, the fluid remains in motion down to lower heat input levels compared to the start-up phase.
- The higher the tilting angle, the higher the heat power input needed to reach the dry out conditions. Increasing the inclination angle, the gravitational force better assists the return of the liquid phase to the evaporator zone, cooling the hottest part of the device also for the highest heat power input tested.
- At very high heat power inputs (above 180 W), the fluid motion follows a preferential direction. This is likely due to little asymmetries of the experimental apparatus, leading to speculate that by designing a device with a deliberate increase of asymmetry (for example, by wrapping the electrical wires only on one side of the U-turns), the fluid flow motion could follow a preferential direction, stabilizing the fluid flow motion and also increasing thermal performance.

NOMENCLATURE

Δh_{lv}	Latent heat of vapor	[J/kg]
g	Gravity Acceleration	[m/s^2]
q''	Heat flux	[W/cm^2]
$\dot{Q}$	Heat Input Power	[W]
R_{eq}	Equivalent Thermal Resistance	[K/W]
T	Temperature	[°C]
ρ_l	Liquid Density	[kg/m^3]
ρ_v	Vapor Density	[kg/m^3]
σ	Surface Tension	[N/m]

ACKNOWLEDGEMENTS

The present work has been carried out in the framework of the Italian Space Agency (ASI) project ESA_AO-2009 entitled "Innovative two-phase thermal control for the International Space Station". The authors would like to thank Dr. Olivier Minster and Dr. Balazs Toth for their interest and support to the PHP activities and for the fruitful discussions. Also we acknowledge Ing. Paolo Emilio Battaglia of the Italian Space Agency for his support. Finally we thank all the members of the Pulsating Heat Pipe International Scientific Team, for their contribution in pushing the

PHP technology for space applications, with a particular gratitude to Prof. Sameer Khandekar, Dr. Vadim Nikolayev, Dr. Vincent Ayel and Prof. Marcia Mantelli.

REFERENCES

Esen, M., Esen, H., 2005, Experimental investigation of a two-phase closed thermosyphon solar water heater, *Sol. Energy*, Vol.79, pp. 459-468.

Franco, A., Filippeschi, S., 2010, Experimental analysis of heat and mass transfer in small dimension, two-phase loop thermosyphons, *Heat Pipe Sci. Technol.*, Vol. 2, pp. 163–182.

Franco, A., Filippeschi, S., 2012, Closed Loop Two-Phase Thermosyphon of Small Dimensions: a Review of the Experimental Results, *Microgravity Sci. Technol*. Vol. 24, pp.165–179.

Franco, A., Filippeschi, S., 2013**,** Experimental analysis of Closed Loop Two Phase Thermosyphon (CLTPT) for energy systems, *Exp. Therm.Fluid Sci.*, Vol. 51, pp. 302–311.

Han, L., Shi, W., Wang, B., Zhang, P., Li, X., 2013, Development of an integrated air conditioner with thermosyphon and the application in mobile phone base station, *Int. J. of Refrigeration*, Vol. 36, pp. 58-69.

Henry, C.D., Kim, J., Chamberlain, B., 2004, Heater size and heater aspect ratio effects on sub-cooled Pool boiling heat transfer in low-g, *3rd International Symposium on Two-Phase Flow Modeling and Experimentation, Pisa, Italy*.

Jouhara, H., Robinson, A. J. 2010, Experimental investigation of small diameter two-phase closed thermosyphons charged with water, FC-84, FC-77 and FC-3283. *Appl. Therm. Eng.*, Vol. 30, pp. 201–211.

Kaminaga, F., Matsumura, K., Horie, R., Takahashi, A, 2012, A Study on Thermal Conductance in a Looped Parallel Thermosyphon, *16th International Heat Pipe Conference*, Lyon, France, pp. 225-231.

Kim, C.J., Yoo, B.O., Park, Y.J. 2005. Experimental Study of a Closed Loop Two-Phase Thermosyphon with Dual Evaporator in Parallel Arrangement, *Journal of Mech. Sci. and Tech*., Vol. 19(1), pp. 189-198.

Lahey, R.T, Moody, F.J., 1993, *Thermal Hydraulic of Boiling Water Nuclear Reactor*, 2nd. Ed., ANS.

Li, J., Lin, F., Niu, G., 2014. An insert-type two-phase closed loop thermosyphon for split-type solar water heaters, Appl. Therm. Eng., Vol.70, pp. 441-450.

Mameli, M., Manno, V., Filippeschi, S., Marengo, M. 2013, Thermal instability of a Closed Loop Pulsating Heat Pipe: Combined effect of orientation and filling ratio, *Exp. Therm. Fluid Sci.*, Vol. 59, pp. 222–229.

Moradgholi, M., Nowee, S.M., Abrishamchi, I., 2014, Application of heat pipe in an experimental investigation on a novel photovoltaic/thermal (PV/T) system, *Sol. Energy*, Vol.107, pp. 82-88.

Perpinà, X., Piton, M,. Mermet-Guyennet, M., Jorda,` X., Millàn, J. 2007. Local thermal cycles determination in thermosyphon-cooled traction IGBT modules reproducing mission profiles, *Microelectron. Reliab.*, Vol. 47, pp. 1701–1706.

Reay, D.A., Kew, P.E., 2006. Heat Pipes, Fifth ed., Butterworth-Heinemann, Burlington, USA, 2006.

Sarno, C., Tantolin, C., Hodot, R., Maydanik, Y., Vershinin, S., 2013. Loop thermosyphon thermal management of the avionics of an in-flight entertainment system, *Appl. Therm. Eng.*, Vol. 51, pp. 764-769.